USING MRI TO STUDY *IN SITU* OIL RECOVERY DURING CO_2 INJECTION IN CARBONATES

Brautaset[1], A., Ersland[1], G., Graue[1], A.,
Stevens[2], J. and Howard[2], J.
[1] Dept. of Physics and Technology, University of Bergen, Norway
[2] ConocoPhillips, Bartlesville, OK, USA

This paper was prepared for presentation at the International Symposium of the Society of Core Analysts held in Abu Dhabi, UAE 29 October-2 November, 2008

ABSTRACT

Fluid flow behavior during enhanced oil recovery experiments in chalk utilizing waterflooding and subsequent injection of CO_2 at miscible conditions was investigated in a n-Decane/deuterium oxide brine system at different wettabilities. During low rate waterflood, fluid saturation distributions were monitored *in situ* as function of time using high spatial resolution Magnetic Resonance Imaging (MRI). At $S_{or,\ D2O}$, CO_2 at either liquid or supercritical conditions was subsequently injected at low flow rate. 3D *in situ* images of the displacement processes indicated that the residual oil after waterflooding was contacted by and mixed with the CO_2 during continued flooding. This caused swelling of the oil phase, oil bank formation and improved sweep efficiency. The EOR potential for the chalk used in these experiments ranged from 17.1 % OOIP to 67.1 % OOIP depending on the wettability and the initial core saturations. Material balance measurements were used to calculate fluid saturations, and the results exhibited improved sweep efficiency and increased oil recovery.

INTRODUCTION

Injection of CO_2 in mature oil fields has proven to be an efficient EOR method due to its miscibility properties at high pressures and its ability to increase the mobility of the oil phase. In fractured carbonate reservoirs, parameters such as matrix permeability, wettability, reservoir pressure and temperature, initial water saturation, fracture-matrix geometry, production rates and oil and solvent viscosities and densities have great impact on oil recovery and sweep efficiency (Li (2000), Slobod (1964), Thompson (1969), Firoozabadi (1994), Jamshidnezhad (2004), Holm (1986), Asghari (2008)). Due to the complexity of the recovery mechanisms involved during CO_2 injection, the need for *in situ* data is of great importance in order to fully understand the displacement process.

In this study, waterfloods and subsequent CO_2 injections in low-permeable chalk at different wettabilities have been conducted at either liquid or supercritical conditions and above the reported Minimal Miscibility Pressure (MMP) for the system to ensure miscibility with the oil phase. High spatial resolution Magnetic Resonance Imaging (MRI)

has been utilized to calculate fluid saturations and to qualitatively monitor the displacement processes. The main objective of the study was to investigate the displacement process *in situ* and to determine the enhanced oil recovery potential from the CO_2 injection. A part of the study was to compare the effects from using supercritical CO_2 and liquid CO_2 and to study the *in situ* effects from injecting CO_2 at S_{wi} and $S_{or, D2O}$.

EXPERIMENTAL

Four 3.81 cm diameter Portland Chalk core samples were oven dried for two days at 90°C, evacuated and saturated with synthetic brine. Porosity was calculated from weight measurements and absolute permeability to brine was measured using a Hassler type core holder. Three of the cores were drained to S_{wi} and aged using low rate injection of North Sea light crude oil at 80°C for selected periods of time to reach less water-wet and neutral-wet conditions. A more detailed description of the Portland chalk is found in Ekdale (1993), and the ageing process is described in Graue (1999), Graue (2002) and Aspenes (2003). One core was left at strongly water-wet conditions. Basic core properties, including length, diameter, porosity, absolute permeability to brine and Amott Indices after ageing are listed in Table 1.

Table 1. Core Properties.

Core Name	Length [cm]	Diameter [cm]	Porosity [%]	Permeability [mD]	Amott Index [frac.]
P1	10.02	3.81	48.4	3.96	0.29
P2	10.02	3.80	47.9	4.61	0.25
P7	10.00	3.81	48.4	3.56	1.00
G23	6.01	3.80	47.6	4.30	0.15

The four core samples were prepared for the MRI experiments by substituting brine with deuterium oxide brine in order to distinguish the water phase from the oil phase in the MRI, and thus the measured MRI intensities during waterfloods could be related to oil saturation. The cores were finally drained with n-Decane to reach S_{wi}. Fluid properties, including brine compositions and densities and viscosities at relevant temperatures and pressures are listed in Table 2.

The critical point of CO_2 is at 31.1 °C and 7398 kPa. Minimum Miscible Pressure (MMP) for the n-Decane/CO_2 system has been determined at 35 °C and 7329 kPa by Asghari (2008) and at 37.8 °C and 7894 kPa by Ayirala (2005). To ensure liquid properties of CO_2, the temperature and pressure were selected at 23 °C and 8274 kPa, respectively. To ensure supercritical properties, temperature and pressure were selected to 40 °C and 8274 kPa, respectively. All injection rates were set to 2 ml/h, corresponding to a frontal velocity of approximately 0.2 ft/d, to minimize fingering effects (Rathmell (1971)).

Table 2. Fluid Properties.

Fluid	Brine	D_2O Brine	Crude oil	n-Decane	CO_2
Composition	5.0 wt% NaCl 3.8 wt% $CaCl_2$ 0.1 wt% NaN_3	5.0 wt% NaCl 3.8 wt% $CaCl_2$	-	-	-
Density [g/cm^3] at 20°C	1.05	1.18	0.85	0.73	0.002
Density [g/cm^3] at 8274 kPa, 40°C	-	-	-	0.72	0.314
Viscosity [cP] at 20°C	1.09	1.10	14.3	0.92	0.015
Viscosity [cP] at 8274 kPa, 40°C	-	-	-	0.76	0.024
Viscosity [cP] at 80°C	-	-	2.7	-	-

During low rate, high pressure waterflood and subsequent injection of either liquid or supercritical CO_2 in three of the core samples, Magnetic Resonance Imaging (MRI) was used

1) to image fluid saturation distributions *in situ*, and
2) to investigate oil recovery mechanisms *in situ*.

In one core sample, supercritical CO_2 was injected at S_{wi}. Table 3 summarizes the Amott indices and the initial oil saturations of the core samples and the injection properties of the CO_2.

Table 3. Injection Data.

Core Name	Amott Index	$S_{o,wi}$ [%]	Temperature [°C]	CO_2 State	CO_2 Injection
P1	0.29	80.1	40	Supercritical	S_{wi}
P2	0.25	75.0	40	Supercritical	$S_{or,\ D2O}$
P7	1.00	69.8	23	Liquid	$S_{or,\ D2O}$
G23	0.15	79.9	23	Liquid	$S_{or,\ D2O}$

Figure 1 shows a schematic of the experimental setup. The core holder was installed horizontally in the MRI and connected to the two injection pumps and a third pump controlling the confining pressure. The pumps were operated by a laptop computer, and output pressures, injection rates, injected volumes and temperature were logged continuously. The outlet end of the core holder was connected to a fraction collector through a back pressure regulator, allowing the system to be pressurized.

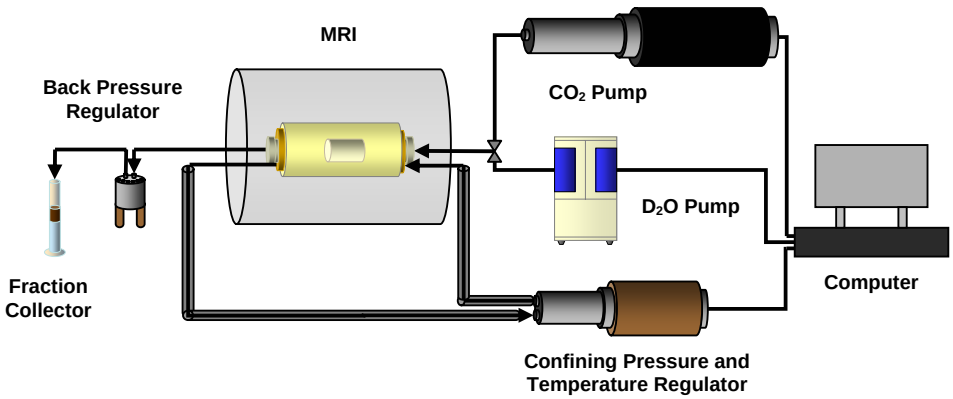

Figure 1: A schematic of the experimental setup.

RESULTS AND DISCUSSION

Table 4 lists initial and endpoint oil saturations and recovery factors from the waterfloods and CO_2 injections. From the table, injection of supercritical CO_2 at S_{wi} (in core plug P1) yields the lowest total recovery (67.1 % OOIP) of the four core samples. The most efficient oil recovery, 93.6 % OOIP, was obtained by waterflooding followed by CO_2 injection at supercritical conditions in the less water-wet core plug P2.

Table 4. Production Data.

Core Name	P1	P2	P7	G23
Amott Index	0.29	0.25	1.00	0.15
$S_{o, wi}$ [% PV]	80.1	75.0	69.8	79.9
$S_{or, D2O}$ [% PV]	-	26.9	25.2	53.2
$S_{w, or, D2O}$ [% PV]	-	73.1	74.8	46.8
$R_{f, D2O}$ [% OOIP]	-	64.1	63.9	33.4
$S_{or, CO2}$ [% PV]	26.4	4.8	13.3	20.3
$S_{w, or, CO2}$ [% PV]	24.6	59.0	47.0	22.7
$R_{f, CO2}$ [% OOIP]	67.1	29.5	17.1	41.2
$R_{f, total}$ [% OOIP]	67.1	93.6	81.0	74.6

Injection of supercritical CO_2 at $S_{or, D2O}$ at less water-wet conditions (core plug P2) provides the lowest $S_{or, CO2}$ (4.8 % PV) and proves to be the most efficient production strategy compared to injection of liquid CO_2 at $S_{or, D2O}$ at strongly water-wet conditions (core plug P7 with $S_{or, CO2}$ at 13.3 % PV) and to injection of liquid CO_2 at $S_{or, D2O}$ at near neutral-wet conditions (core plug G23 with $S_{or, CO2}$ at 20.3 % PV). Total oil recovery from injection of liquid CO_2 at $S_{or, D2O}$ is 81.0 % OOIP at strongly water-wet conditions (core plug P7) and 74.6 % OOIP at near neutral-wet conditions (core plug G23).

Figure 2 shows 2D and 3D MRI images of the oil saturation dynamics during injection of supercritical CO_2 at S_{wi} as function of injected pore volumes in the less water-wet core plug P1. The bright areas (yellow and red) indicate high oil saturation, and the dark areas (blue) indicate low oil saturation. The effluent production from D_2O injection (red line) and from CO_2 injection (black line) at each time step is indicated by the average oil saturation development in the core in the lower left corner of each time step. The injection of CO_2 causes swelling of the oil phase, seen as bright green and red areas near the inlet end in image 2, 3 and 4. The CO_2 enters the core in a piston-like displacement, leaving the residual oil and water saturations behind the CO_2 front.

Figure 3 and Figure 4 show 2D and 3D MRI images of the oil saturation dynamics during waterflood (red) and the following injection of supercritical CO_2 (black) in the less water-wet core P2, respectively. The waterflood images in Figure 3 show that the water enters the core in a piston-like displacement, leaving residual oil saturation of 26.9 % PV. MRI intensity as function of oil saturation during a waterflood in a water-oil system does not show the same non-linear response as for the water-oil-CO_2 system. Thus, the MRI signal does not disappear as in Figure 2. From Figure 4 oil swelling is observed as a bright green area moving through the core as the CO_2 enters the core, leaving a residual oil saturation of 4.8 % PV.

Figure 5 and Figure 6 show 2D and 3D MRI images of the oil saturation dynamics during waterflood and subsequent injection of liquid CO_2 in the near neutral-wet core sample G23, respectively. Minor fingering effects in the 2D images and an evenly distributed decrease in oil saturation is observed in Figure 5 during waterflooding. The high $S_{or,\ D2O}$ of 53.2 % PV is due to the early termination of the waterflood. Figure 6 shows swelling of the oil phase, piston-like displacement and loss of MRI signal during injection of CO_2, leaving a residual oil saturation of 20.3 % PV.

In the last images of the CO_2 injection sequences, the signal disappears behind the CO_2 front, but material balance indicates residual oil saturation of 26.4 % PV, 4.8 % PV and 20.3 % PV for the core plugs P1, P2 and G23, respectively. The absence of MRI signal is likely due to changes in the relaxation properties in the oil phase when mixing with CO_2. Preliminary experiments indicate that there is a non-linear MRI response of signal intensity to oil saturation as the CO_2 content increases that may reflect changes in oil T_1 values. The MRI signal during waterflood, however, is unaffected by the CO_2 effect on the oil signal and should provide a qualitative comparison with the mass balance estimates of saturations. The uncertainty at this time in the MRI properties of the oil-CO_2 mixtures does not allow for reproducible predictions of saturation during the CO_2 flooding process as evident in the variations that appear amongst the different core samples in this study. Additional measurements on oil-CO_2 MRI properties are needed before quantitative information from the images during CO_2 flood can be extracted.

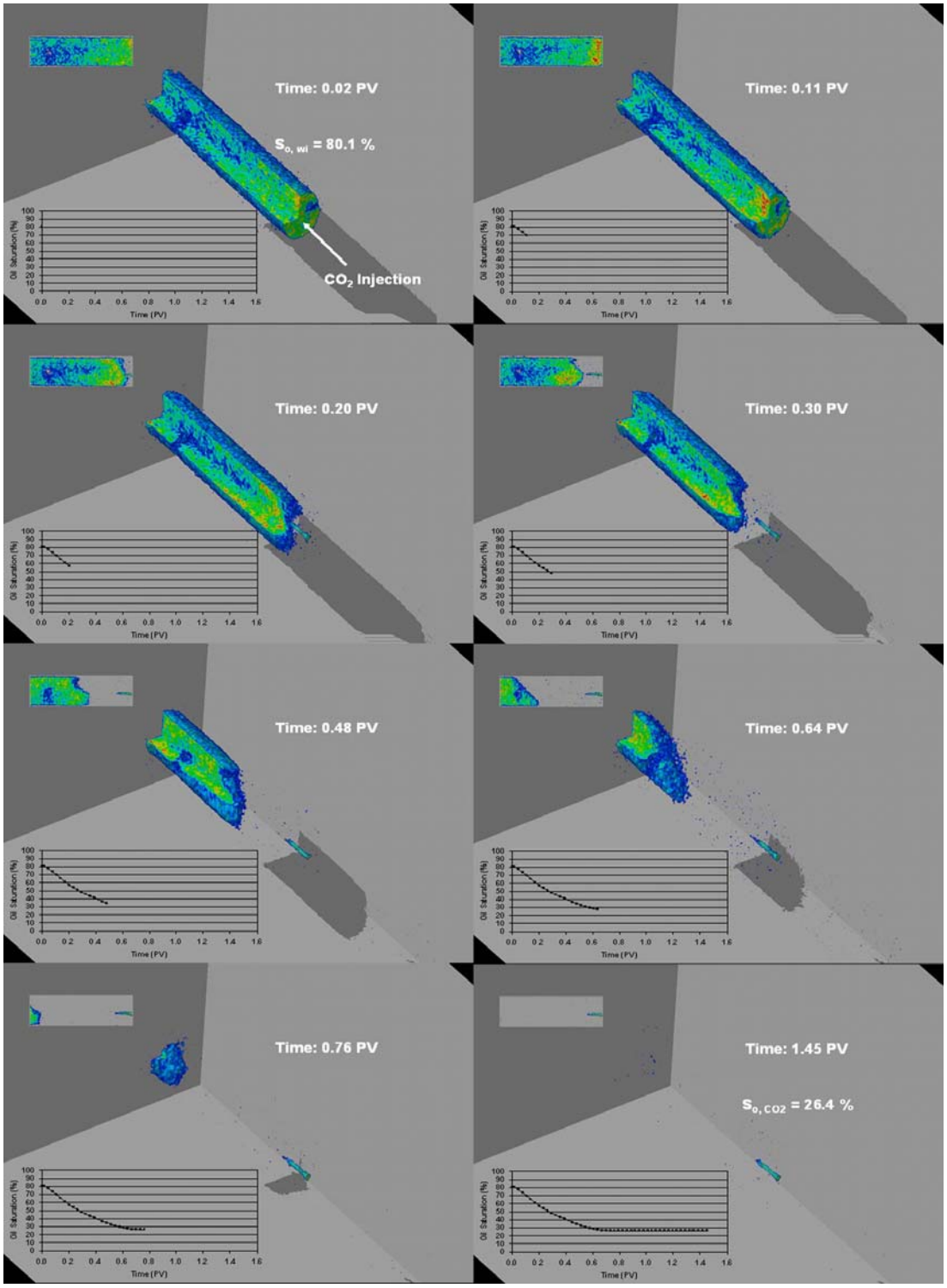

Figure 2. Supercritical CO_2 injection at S_{wi} in the less water-wet core sample P1.

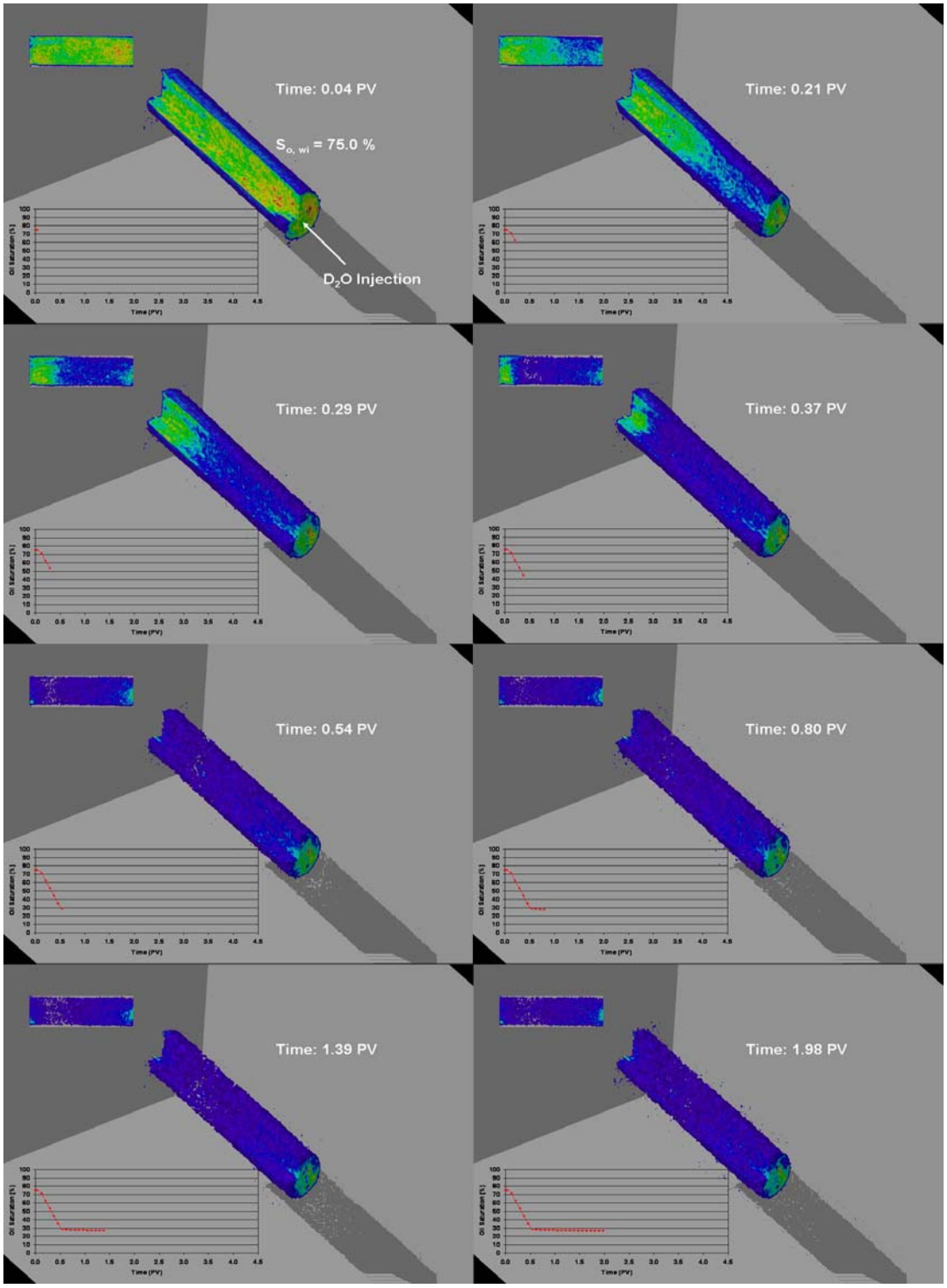

Figure 3. Waterflood of the less water-wet core sample P2.

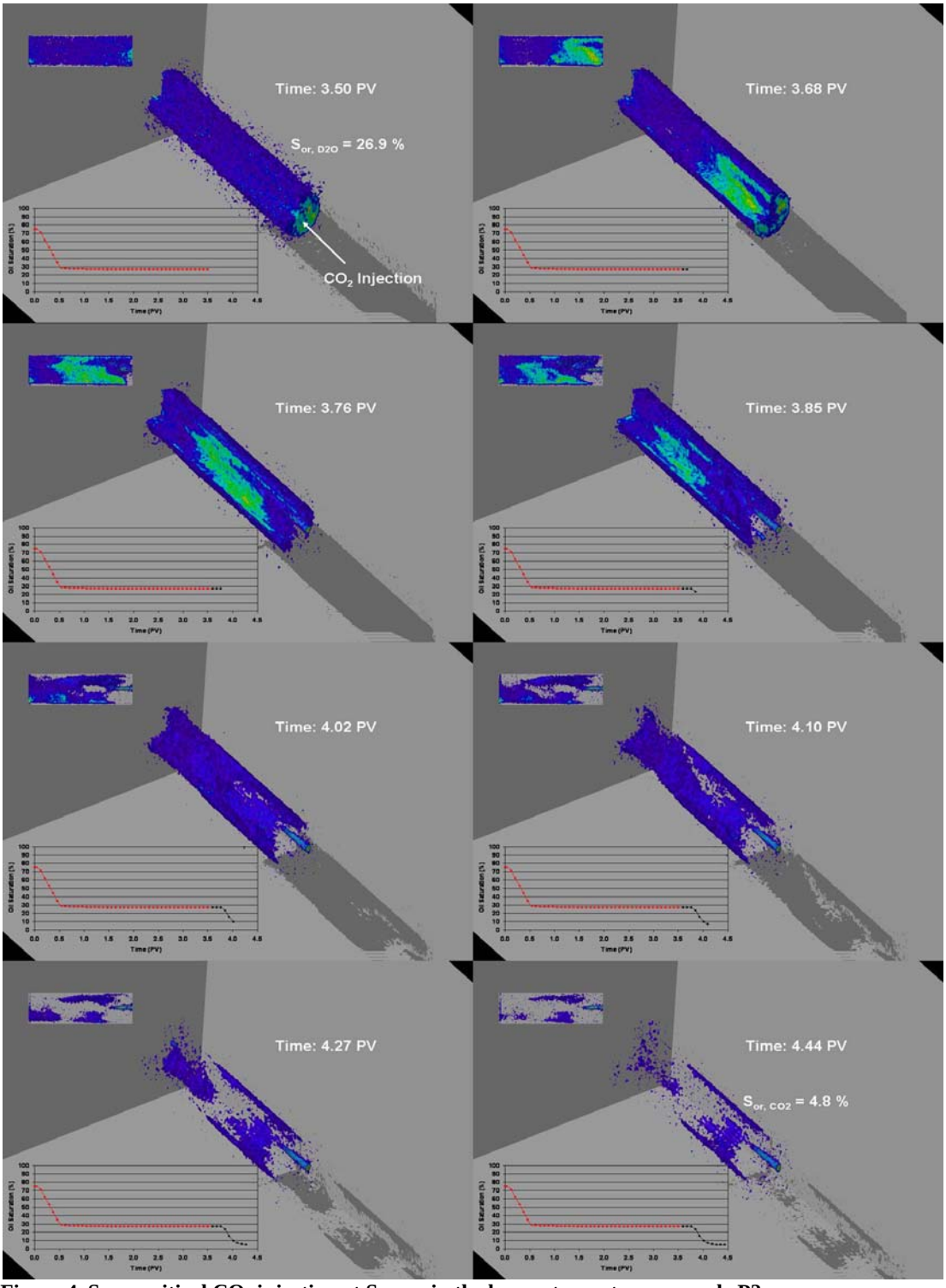

Figure 4. Supercritical CO_2 injection at $S_{or, D2O}$ in the less water-wet core sample P2.

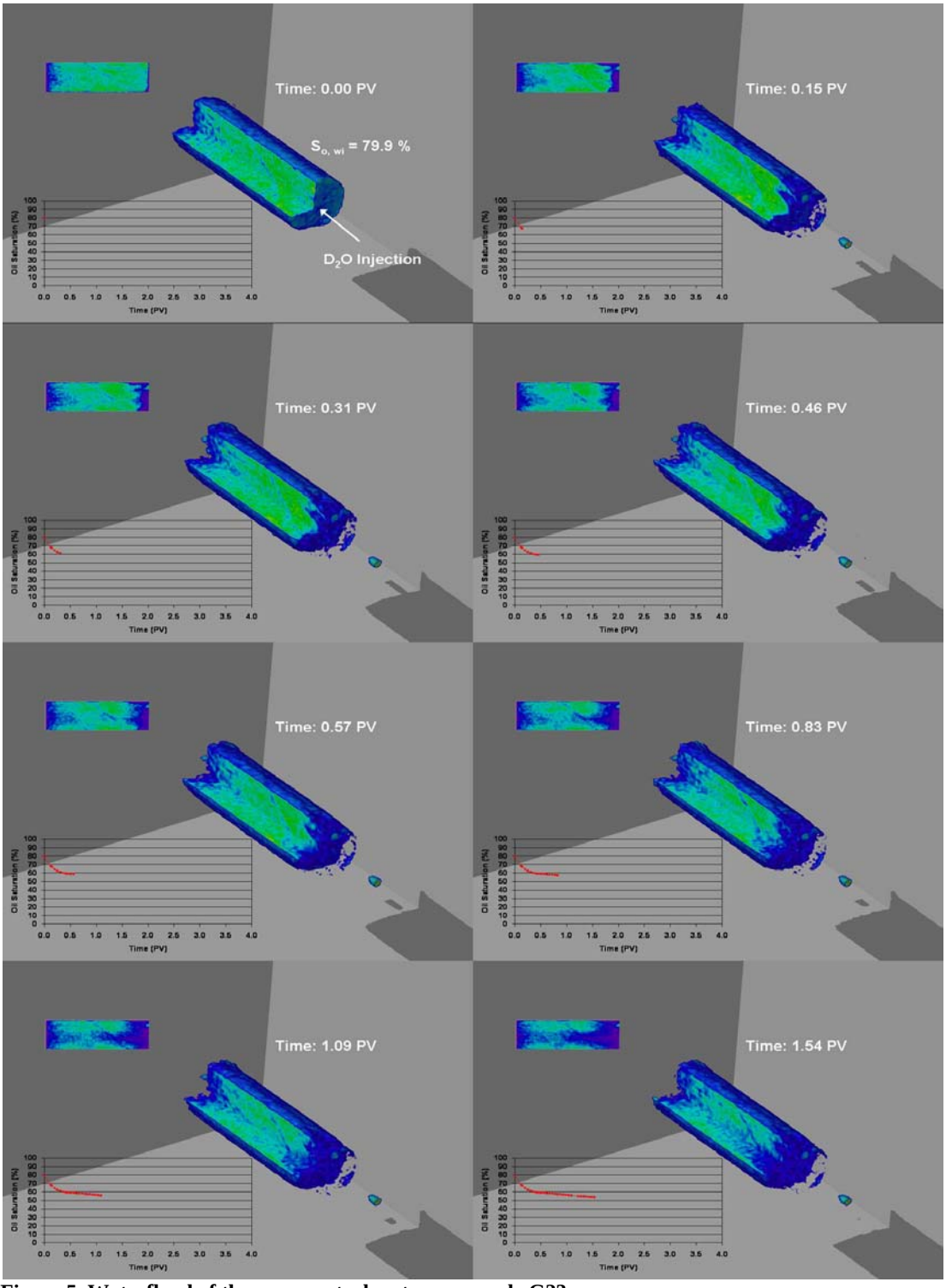

Figure 5. Waterflood of the near neutral-wet core sample G23.

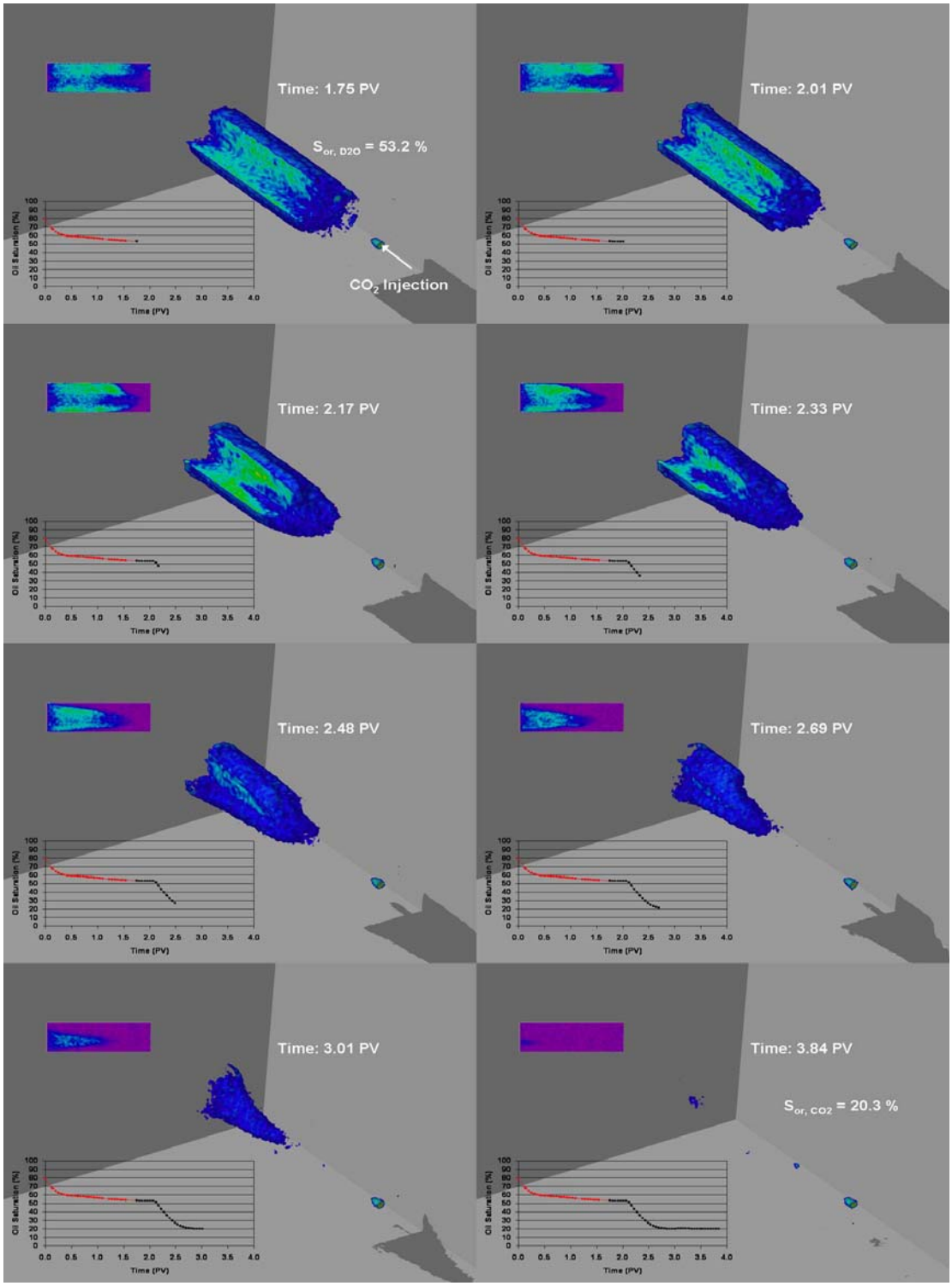

Figure 6. Liquid CO_2 injection at $S_{or, D2O}$ in the near neutral-wet core sample G23.

CONCLUSIONS

- Magnetic Resonance Imaging was used to investigate fluid saturation distributions and to monitor the fluid flow characteristics *in situ* during waterfloods and subsequent injection of either liquid or supercritical CO_2 in four Portland Chalk core samples at different wettabilities.
- Injection of CO_2 at S_{wi} has a lower total recovery factor compared to a waterflood followed by injection of CO_2 at $S_{or,\ D2O}$.
- Injection of CO_2 at supercritical conditions exhibits higher total oil recovery than similar injection of liquid CO_2.

ACKNOWLEDGEMENTS

One of the authors is indebted for financial support from the Norwegian Research Council. The authors wish to acknowledge ConocoPhillips for permission to publish and for the use of the MRI facilities at the ConocoPhillips Research Center in Bartlesville, OK, USA.

NOMENCLATURE

MMP : Minimum Miscible Pressure
MRI : Magnetic Resonance Imaging
OOIP : Original Oil in Place
$R_{f,\ CO2}$: Recovery Factor from CO_2 Injection
$R_{f,\ D2O}$: Recovery Factor from D_2O Injection
$R_{f,\ total}$: Total Recovery Factor
$S_{o,\ wi}$: Oil Saturation at Irreducible Water Saturation
$S_{or,\ CO2}$: Residual Oil Saturation after CO_2 Injection
$S_{or,\ D2O}$: Residual Oil Saturation after D_2O Injection
$S_{w,\ or,\ CO2}$: D_2O Saturation at Residual Oil Saturation after CO_2 Injection
$S_{w,\ or,\ D2O}$: D_2O Saturation at Residual Oil Saturation after D_2O Injection

SI METRIC CONVERSION FACTORS

cP = 10^{-3} Pa · s
mD = $0.9869 \cdot 10^{-12}$ m^2

REFERENCES

1. Asghari, K., Torabi, F.: "Effect of Miscible and Immiscible CO2 Flooding on Gravity Drainage: Experimental and Simulation Results", *SPE/DOE Improved Oil Recovery Symposium*, Tulsa, Oklahoma, USA, 2008.
2. Aspenes, E., Graue, A., Ramsdal, J., "In situ wettability distribution and wetting stability in outcrop chalk aged in crude oil." *Journal of Petroleum Science and Engineering*, (2003) **39**: 337-350.
3. Ayirala, S. C., Xu, W., Rao, D. N.: "Interfacial Behavior of Complex Hydrocarbon Fluids at Elevated Pressures and Temperatures", *International Conference on MEMS, NANO and Smart Systems*, Banff, Alberta, Canada, 2005.
4. Ekdale, A. A., Bromley, R. G.. "Trace Fossils and Ichnofabric in the Kjølby Gaard Marl, Uppermost Creataceous, Denmark." *Bulletin of the Geological Society of Denmark*, (1993) **31**: 107-119.
5. Firoozabadi, A., Markeset, T. I.: "Miscible Displacement in Fractured Porous Media: Part 1 - Experiments", *SPE/DOE Improved Oil Recovery Symposium*, Tulsa, Oklahoma, USA, 1994.
6. Graue, A., Aspenes, E., Bognø, T., Moe, R. W., Ramsdal, J., "Alteration Of Wettability And Wettability Heterogeneity." *Journal of Petroleum Science and Engineering*, (2002) **33**: 3-17.
7. Graue, A., Viksund, B. G., Baldwin, B. A., "Reproducible Wettability Alteration of Low-Permeable Outcrop Chalk." *SPE Reservoir Evaluation and Engineering*, (1999) **2**: 134-140.
8. Holm, L. W., "Miscibility and Miscible Displacement." *Journal of Petroleum Technology*, (1986) **August**: 817-818.
9. Jamshidnezhad, M., Montazer-Rahmati, M., Sajjadian, V. A., "Theoretical and Experimental Investigations of Miscible Displacement in Fractured Porous Media." *Transport in Porous Media*, (2004) **57**: 59-73.
10. Li, K., Firoozabadi, A., "Experimental Study of Wettability Alteration to Preferential Gas-Wetting in Porous Media and Its Effects." *SPE Reservoir Evaluation and Engineering*, (2000) **April**.
11. Rathmell, J. J., Stalkup, F. I., Hassinger, R. C.: "A Laboratory Investigation of Miscible Displacement by Carbon Dioxide", *SPE Annual Fall Meeting*, New Orleans, Louisiana, USA, 1971.
12. Slobod, R. L., "The Effects of Gravity Segregation in Laboratory Studies of Miscible Displacement in Vertical Unconsolidated Porous Media." *SPE Journal*, (1964) **March**: 1-8.
13. Thompson, J. L., Mungan, N., "A Laboratory Study of Gravity Drainage in Fractured Systems Under Miscible Conditions." *SPE Journal*, (1969) **June**: 247-254.